

ThAu₂⁻, ThAu₂O⁻, and ThAuOH⁻ anions: Photoelectron spectroscopic and theoretical characterization

Cite as: J. Chem. Phys. **156**, 054305 (2022); <https://doi.org/10.1063/5.0079795>

Submitted: 24 November 2021 • Accepted: 13 January 2022 • Accepted Manuscript Online: 13 January 2022 • Published Online: 02 February 2022

Zhaoguo Zhu, Mary Marshall,  Kit H. Bowen, et al.



View Online



Export Citation



CrossMark

ARTICLES YOU MAY BE INTERESTED IN

Anion photoelectron spectroscopy and theoretical calculations of Cu₄O_n^{-/0} (n = 1-4):

Identification of stable quasi-square structure for Cu₄O₄⁻

The Journal of Chemical Physics **156**, 054304 (2022); <https://doi.org/10.1063/5.0078415>

Size-dependent Reactivity of Rhodium Deuteride Cluster Anions Rh₃D_n⁻ (n = 0-3) toward Dinitrogen: The Prominent Role of σ Donation

The Journal of Chemical Physics (2022); <https://doi.org/10.1063/5.0077183>

BDF: A relativistic electronic structure program package

The Journal of Chemical Physics **152**, 064113 (2020); <https://doi.org/10.1063/1.5143173>

The Journal
of Chemical Physics

SPECIAL TOPIC: Low-Dimensional
Materials for Quantum Information Science

Submit Today!



ThAu₂⁻, ThAu₂O⁻, and ThAuOH⁻ anions: Photoelectron spectroscopic and theoretical characterization

Cite as: J. Chem. Phys. 156, 054305 (2022); doi: 10.1063/5.0079795

Submitted: 24 November 2021 • Accepted: 13 January 2022 •

Published Online: 2 February 2022



View Online



Export Citation



CrossMark

Zhaoguo Zhu,¹ Mary Marshall,¹ Kit H. Bowen,^{1,a)}  and Kirk A. Peterson^{2,a)} 

AFFILIATIONS

¹Department of Chemistry, Johns Hopkins University, Baltimore, Maryland 21218, USA

²Department of Chemistry, Washington State University, Pullman, Washington 99164, USA

^{a)}Authors to whom correspondence should be addressed: kbowen@jhu.edu and kipeters@wsu.edu

ABSTRACT

The thorium–gold negative ions ThAu₂⁻, ThAu₂O⁻, and ThAuOH⁻ have been observed and experimentally characterized by anion photoelectron spectroscopy. These experiments are accompanied by extensive *ab initio* electronic structure calculations using a relativistic composite methodology based primarily on coupled cluster singles and doubles with perturbative triples calculations. The theoretical electron affinities (EAs) at 0 K agree with the experimental adiabatic EAs to within 0.02 eV for all species. Two separate isomers were located in the calculations for ThAuOH⁻, and detachment from both of these appears to be present in the photoelectron spectrum. Excited electronic states of the neutral molecules are reported at the equation of motion-coupled cluster singles and doubles level of theory. Atomization energies and heats of formation are also calculated for each neutral species and have expected uncertainties of 3 and 4 kcal/mol, respectively. The σ bonds between Th and Au are determined by natural bond orbital analysis to consist of predominately sd hybrids on Th bonding with the Au 6s orbital. In order to investigate the correspondence between the bonding in Th–Au and Th–F molecules, a limited number of calculations were also carried out on most of the F-analogs of this study. These results demonstrate that Au does behave like F in these cases, although the Th–F σ bonds are much more ionic compared to Th–Au. This results in an EA for ThF₂ that is 10 kcal/mol smaller than that of ThAu₂. The EA values for the Th(IV) species, i.e., ThX₂O and ThXOH, only differed, however, by 3–4 kcal/mol.

Published under an exclusive license by AIP Publishing. <https://doi.org/10.1063/5.0079795>

I. INTRODUCTION

The chemistry of actinides (An's) has received prodigious attention in recent years due to the wide applications of uranium and plutonium in nuclear energy development.¹ The renewed research on the thorium-based molten salt fast reactors (MSFRs) shows that thorium, the second element in the An series, is a potential nuclear fuel to complement uranium-based reactors.^{2–4} In addition, the high natural abundance of thorium (9.6 ppm) in the Earth's crust compared to that of uranium (2.7 ppm) is an economic stimulus to the development of the next-generation nuclear reactor.⁴ Thorium is an early An element without 5f electrons and has an atomic ground-state electron configuration of [Rn]6d²7s², analogous to group IV transition metals. Owing to the significant relativistic and non-negligible electron correlation effects, electronic structures of

thorium-containing compounds are complicated and challenging for theoretical calculations.^{5–10} The combination of experimental data and calculations is vital for interpreting and understanding thorium chemistry.

Gold–thoria catalysts, which are ThO₂-supported on gold clusters or a single gold atom, showed extremely high catalytic activity for carrying out the water–gas shift reaction (WGS) and the process of CO oxidation.^{11–13} Tabakova *et al.* (2006) suggested that the WGS activity is related to the gold clusters interacting with thoria.¹¹ Notably, an OH group probably at the boundary of the gold–thoria catalyst may interact with CO resulting in a formate intermediate toward the formation of CO₂, which means that the Au_x–Th_yO_nH (x, y, n = 0, 1, 2, 3, . . .) moiety in the catalyst plays a critical role in the CO oxidation reaction. Although several first principle calculations were performed to study the mechanism of CO

oxidation by gold–thoria catalysts, the function of the OH group is unexplored at the molecular level.^{12,13} To give a better understanding of the structure of the gold–thoria catalyst, it is essential to study the chemical bonding in thorium–gold, thorium–gold oxide, and thorium–gold hydroxide species.

In addition to the bulk thorium–gold containing species, small thorium–gold and thorium–gold oxide clusters are also of great interest to theorists. Barysz and Pyykkö performed a first principle theoretical study of the ThAu^+ cation, identified its $^1\Sigma^+$ ground state, and showed that it has a single bond with a bond dissociation energy of 3.5 eV.¹⁴ In 2006, Pyykkö's theoretical work reported that ThAu_2^{2+} and OThAu^+ have $D_{\infty h}$ and $C_{\infty v}$ symmetry, respectively.¹⁵ In both ThAu_2^{2+} and OThAu^+ clusters, Au^+ is an analog to oxygen. Additionally, Gagliardi predicted a tetrahedral ThAu_4 cluster in which gold carries a formal charge of $-1|e|$ and behaves like a halogen.¹⁶ The unique properties of Au have been summarized on Cs^+Au^- and $[\text{Au}=\text{C}=\text{Au}]^{2+}$ as well as many other systems.^{17–19} However, experimental studies of thorium–gold clusters are scarce. Recently, the photoelectron spectra of Th_2Au^- and $\text{Th}_2\text{AuO}_{1,2}^-$ were reported by some of the current authors.²⁰ Those experiments were also accompanied by *ab initio* calculations similar to those of this study. To the best of our knowledge, no experimental or theoretical data have been reported on the structures and bonding of $\text{ThAu}_2^{0/-}$, $\text{ThAu}_2\text{O}^{0/-}$, or $\text{ThAuOH}^{0/-}$ clusters.

In this paper, we report the first investigation on ThAu_2^- , ThAu_2O^- , and ThAuOH^- anions in the gas phase using photoelectron spectroscopy combined with high level theoretical calculations. Experimental and theoretical results are compared and utilized to characterize the electronic structures and chemical bonding of all three species.

II. METHODS

A. Experimental

The present work utilized anion photoelectron spectroscopy (aPES) as its primary probe. The experimental technique, aPES, is conducted by crossing a mass-selected beam of negative ions with a fixed-energy photon beam and energy analyzing the resulting photodetached electrons. This technique is governed by the energy-conservation relationship, $h\nu = \text{EBE} + \text{EKE}$, where $h\nu$, EBE, and EKE are the photon energy, the electron binding (transition) energy, and the electron kinetic energy, respectively. Our photoelectron spectrometer, which has been described previously,²¹ consists of one of several ion sources, a linear time-of-flight (TOF) mass spectrometer, a mass gate, a momentum decelerator, a neodymium-doped yttrium aluminum garnet (Nd:YAG) laser for photodetachment, and a magnetic bottle electron energy analyzer. Photoelectron spectra were calibrated against the well-known photoelectron spectrum of Cu^- .²²

The anions of interest were generated using a pulsed-arc (discharge) cluster ionization source (PACIS), which has been described in detail elsewhere.^{23,24} This cluster anion source has been used to generate a variety of bimetal cluster anions.^{25,26} During PACIS operation, a 30 μs long, 150-V electrical pulse applied across the Cu anode and the Th–Au sample cathode in the discharge chamber vaporizes the Th and Au atoms. The sample cathode had been prepared in a nitrogen glove box, where a Th–Au powder mixture was firmly pressed onto a copper rod. Another layer of Cu powder was

pressed onto the top of the Th–Au layer to prevent contact between the thorium powder and air. Almost simultaneously with the electrical discharge, 150 psi of ultrahigh purity helium gas was injected into the discharge region to make the ThAu_2^- and ThAu_2O^- anions, while 150 psi of pure hydrogen gas was used to make the ThAuOH^- anion. The resulting mixture of atoms, ions, and electrons then reacted and cooled as it expanded through the PACIS housing and nozzle. The resultant anions were further analyzed by TOF mass spectroscopy and aPES.

B. Computational

Equilibrium geometries of all six species ($\text{ThAu}_2/\text{ThAu}_2^-$, $\text{ThAu}_2\text{O}/\text{ThAu}_2\text{O}^-$, and $\text{ThAuOH}/\text{ThAuOH}^-$) were optimized at the coupled cluster singles and doubles with perturbative triples, CCSD(T), level of theory.²⁷ For the open-shell anion species, restricted open-shell Hartree–Fock (ROHF) orbitals were used in CCSD(T) calculations where the spin restriction is relaxed in the CCSD solutions, i.e., R/UCCSD(T).²⁸ For these geometry optimizations, the third-order Douglas–Kroll–Hess (DKH3) scalar relativistic Hamiltonian^{29–32} was used throughout with diffuse-augmented correlation consistent basis sets from double- to triple-zeta ($n = \text{D}, \text{T}$), i.e., aug-cc-pVnZ-DK for O and H,^{33,34} the newly developed aug-cc-pVnZ-DK3 for Au,³⁵ and the cc-pVnZ-DK3 sets^{36,37} for Th augmented by a diffuse function in each angular symmetry obtained via even-tempered extension. Throughout this text, these basis sets will be denoted as aVnZ ($n = \text{D}, \text{T}$, and Q). In these calculations, only the valence electrons were correlated (6s6p6d7s for Th, 6s5d for Au, 2s2p for O, and 1s for H), i.e., the standard frozen-core (FC) approximation was employed.

The CCSD(T) equilibrium geometries calculated at the triple-zeta level were then used in subsequent Feller–Peterson–Dixon (FPD) composite calculations^{37–40} of the electron affinities and atomization energies, with the latter leading to heats of formation. Specifically, the FPD energy is defined in this work to be

$$E_{\text{FPD}} = E_{\text{FC-CCSD(T)/aVQZ}} + \Delta E_{\text{CBS}} + \Delta E_{\text{CV}} + \Delta E_{\text{QED}} + \Delta E_{\text{SO}} + \Delta E_{\text{ZPE}}. \quad (1)$$

On the right-hand-side of Eq. (1), $E_{\text{FC-CCSD(T)/aVQZ}}$ is the frozen-core DKH3 CCSD(T) energy calculated with the aVQZ basis set. The complete basis set (CBS) limits were obtained using core–valence basis sets, aug-cc-pwCVQZ-DK3 on Au,³⁵ aug-cc-pwCVQZ-DK on O,⁴¹ aug-cc-pVQZ-DK on H,⁴² and diffuse augmented cc-pwCVQZ-DK3 on Th.^{36,37} These sets will be denoted as aCVnZ below ($n = \text{T}, \text{Q}$). Using FC DKH3 CCSD(T) calculations with aCVTZ and aCVQZ basis sets, the HF energies were extrapolated to the HF limit via⁴³ ($n = 3$ and 4 for T and Q, respectively)

$$E_n = E_{\text{CBS}} + A(n+1)e^{6.57\sqrt{n}}, \quad (2)$$

while the CCSD(T) correlation energies were extrapolated with^{44,45}

$$E_n = E_{\text{CBS}} + \frac{B}{(n + \frac{1}{2})^4}. \quad (3)$$

The second term on the right-hand-side of Eq. (1), ΔE_{CBS} , is the difference between the extrapolated CBS limit [sum of the results of Eqs. (2) and (3)] and the aVQZ energy.

The term ΔE_{CV} is the effect of correlating the outer-core electrons, i.e., 5s5p5d on Th, 5s5p on Au, and 1s on O. This is calculated as the difference between DKH3 CCSD(T) calculations with outer-core correlated and frozen core, both with the same aCVTZ and aCVQZ basis sets. These differences were then extrapolated to the CBS limit via Eq. (3).

Small effects due to the leading contribution of QED, the Lamb shift ΔE_{QED} , were obtained using the local model potential approach proposed by Pyykkö and Zhao for the self-energy term, including a fit to the Uehling potential for the vacuum polarization.^{37,46} These calculations were carried out at the frozen-core DKH3-CCSD(T) level of theory with aCVDZ basis sets.

The spin-orbit correction, ΔE_{SO} , was calculated using four-component (4-c) or two-component (2-c) CCSD(T) using orbitals/spinors from average of configuration Dirac-Hartree-Fock (AoC-DHF) calculations. The Dirac-Coulomb-Gaunt (DCG) Hamiltonian and Dyal's spin-free (SF) Hamiltonian⁴⁷ were used throughout using the same aVDZ basis sets defined above but completely uncontracted and with a finite-nucleus model.⁴⁸ It should be noted that the Gaunt term was only implemented at the DHF level of theory. Only valence electrons were correlated in these coupled cluster calculations with virtual orbital cutoffs of 20 E_h . In the cases of $\text{ThAu}_2/\text{ThAu}_2^-$ and $\text{ThAuOH}/\text{ThAuOH}^-$, the SO correction was calculated as the difference between a 4-c CCSD(T) calculation⁴⁹ with the DCG Hamiltonian and one with Dyal's SF Hamiltonian. For the larger $\text{ThAu}_2\text{O}/\text{ThAu}_2\text{O}^-$ pair, the exact 2-c molecular mean field (X2C-mmf) CCSD(T) method⁵⁰ (originating from a DHF calculation with the DCG Hamiltonian) was utilized in place of 4-c CCSD(T). In all cases, the spin-orbit corrections were calculated at the DKH3 CCSD(T)/aVTZ geometries. The SO contribution for the O atom was obtained from its experimental energy levels,⁵¹ with its Gaunt contribution calculated at the AoC-DHF/aVDZ level of theory. Excited electronic states for the neutral molecules were calculated using the equation-of-motion (EOM) CCSD method with the X2C-mmf Hamiltonian (both SF and DCG).^{52,53}

For the calculation of adiabatic electron affinities and atomization energies, zero-point energy (ZPE) corrections were obtained from harmonic vibrational frequencies calculated at the DKH3 CCSD(T) level of theory with the aVDZ basis set throughout except for $\text{ThAu}_2/\text{ThAu}_2^-$, which utilized aVTZ.

Heats of formation at 298 K were calculated by combining FPD atomization energies using the contributions of Eq. (1) for the molecules and atoms, including thermal corrections via standard gas phase partition function expressions, with the known 298 K enthalpies of formation for the gaseous elements: $\Delta H_f(\text{H}) = 52.1028 \pm 0.0000$ kcal/mol, $\Delta H_f(\text{O}) = 59.5672 \pm 0.0005$ kcal/mol,⁵⁴⁻⁵⁶ $\Delta H_f(\text{Au}) = 88.05 \pm 0.26$ kcal/mol,⁵⁷ and $\Delta H_f(\text{Th}) = 143.9 \pm 1.4$ kcal/mol.^{58,59}

Natural Bond Orbital (NBO) analysis,⁶⁰ including natural population analysis (NPA),⁶¹ was carried out with the NBO7 program⁶² using DKH3 Hartree-Fock/aVTZ wave functions. In these calculations, the Th 6s and 6p orbitals were included in the valence space. Nearly all the calculations of this work were carried out with MOLPRO 2020.2,⁶³⁻⁶⁵ except for the SO calculations, which were completed with DIRAC19.⁶⁶

III. RESULTS AND DISCUSSION

A. Experimental results

Figure 1(a) presents the mass spectrum of anionic products ranging from 100 to 900 amu using a 1:1 thorium-gold mixture and helium backing gas. Three major series of clusters are observed. The first series starting from 254 amu consists of ThC_xO_y^- ($x = 0, 1, 2, y = 1, 2$) anion clusters, and the second series beginning from 457 amu is composed of the ThAuAl^- anion and its oxides. The ThAu_2^- anion appears at 626 amu at the beginning of the third series in which we also observe ThAu_2O^- and ThAu_2Al^- anions. Aluminum, as well as carbon and oxygen, is from the surface of the cathode and surroundings in the PACIS source housing. From Fig. 1(b), the ThAuOH^- anion is observed when using 3:1

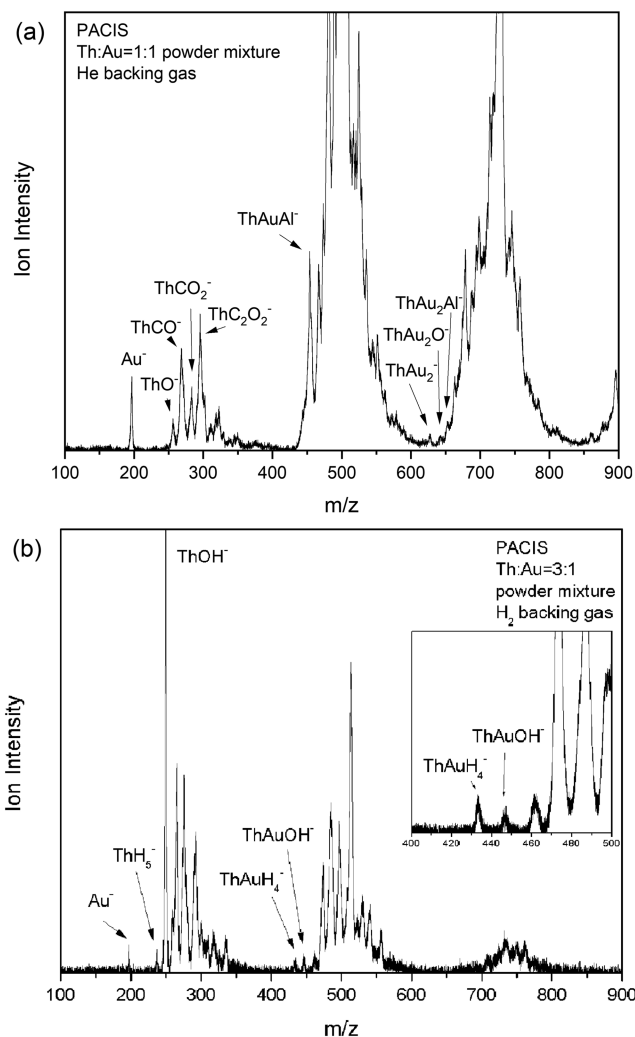


FIG. 1. The mass spectrum of anions generated by the PACIS when using (a) 1:1 thorium-gold mixture and helium gas and (b) 3:1 thorium-gold mixture and hydrogen gas.

thorium–gold mixture and hydrogen gas. We see a variety of thorium hydride anions, thorium hydroxide, thorium–gold hydride, and thorium–gold hydroxide anions in the spectrum in Fig. 1(b).

We, then, applied anion photoelectron spectroscopy with a 355 nm laser to characterize the ThAu_2^- , ThAu_2O^- , and ThAuOH^- anions. The resulting photoelectron spectra of ThAu_2^- , ThAu_2O^- , and ThAuOH^- are presented in Fig. 2. In each spectrum, we observe several peaks corresponding to transitions from the ground state of the anion to different states of its corresponding neutral. For ThAu_2^- , two broad electron binding energy (EBE) bands range from ~ 1.3 to 3.49 eV; they reach their intensity maximum at 1.53 and 2.71 eV. For ThAu_2O^- , the spectrum displays three EBE bands starting from ~ 1.3 , ~ 2.0 , and 2.5 eV, with these attaining their maxima at 1.65 , 2.21 , and 2.73 eV, respectively. In ThAuOH^- 's spectrum, the first feature X, with its threshold occurring at an EBE of ~ 0.7 eV, is peaked at 1.03 eV. Band A, which is the most intense feature in the spectrum, exhibits an onset of signal at 1.23 eV and reaches maximum intensity at 1.43 eV. Band B, which ranges from EBE ~ 2.7 – 3.4 eV, is relatively broad and weak, suggesting that it contains multiple transitions, some of which may be due to multi-electron processes with low transition efficiencies. In the anion photoelectron spectra, the intensity maxima of these peaks represent transitions from the ground state of the anion to the ground and excited states of the neutral counterpart. Among these transitions, the electron

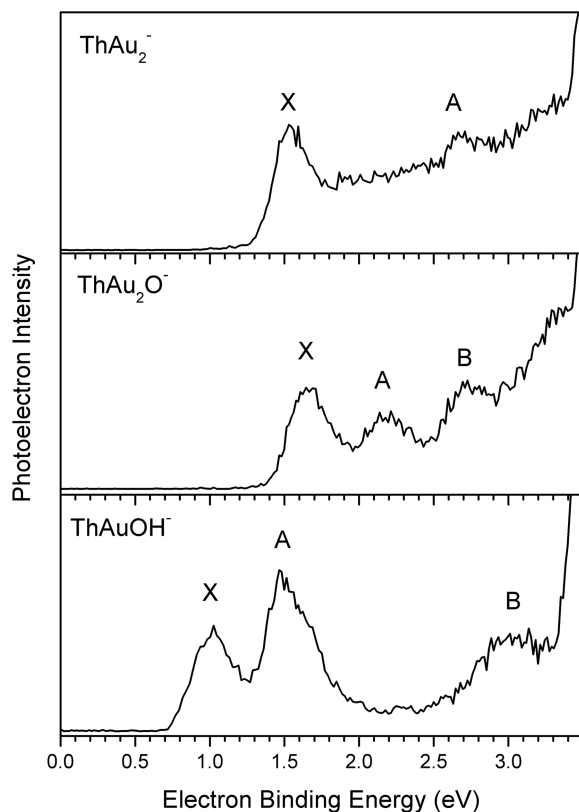


FIG. 2. Photoelectron spectra of ThAu_2^- , ThAu_2O^- , and ThAuOH^- measured with 355 nm (3.49 eV) photons.

binding energy (EBE) value at the peak position in the lowest EBE spectral feature (labeled as X) is the vertical detachment energy (VDE), which is the energy difference between the ground state anion and its neutral counterpart at the geometry of the anion. Thus, VDEs of ThAu_2^- , ThAu_2O^- , and ThAuOH^- are 1.53 , 1.65 , and 1.03 eV, respectively. When there is sufficient Franck–Condon overlap between the ground state of the anion and the ground state of the neutral and when vibrational hot bands are absent, the threshold EBE (E_T) is the value of the electron affinity (EA). Nevertheless, since vibrational temperatures for anions are difficult to estimate and since some degree of vibrational excitation is not uncommon (giving rise to hot bands), the EA value often lies between the threshold and the VDE value. As a reasonable approximation, one can estimate the EA as that corresponding to the EBE value at $\sim 10\%$ of the rising photoelectron intensity. Therefore, EAs of ThAu_2^- , ThAu_2O^- , and ThAuOH^- are evaluated to be 1.30 , 1.35 , and 0.80 eV, respectively. The EA values of ThAu_2^- and ThAu_2O^- are relatively similar to each other, while the EA and VDE values of ThAuOH^- are significantly lower than those of the other two species.

B. Computational results

1. Assignment of low-lying detachment energies

a. $\text{ThAu}_2/\text{ThAu}_2^-$. As shown graphically in Fig. 3 and more specifically in Table I, the ThAu_2 molecule, which has a closed-shell 1A_1 ground state in the absence of SO coupling effects (more on this is discussed below), has a bent, symmetrical structure with a CCSD(T)/aVQZ bond angle of 136.6° . Initial calculations also investigated the presence of low-lying triplet states, which uncovered 3A_1 and 3B_1 states that arise from single excitations from the $7s$ orbital on Th to $6d$ orbitals that correspond to $6d_\delta$ at linear geometries. At the CCSD(T)/aVTZ level of theory, these triplets lie just 2.54 and 2.25 kcal/mol, respectively, above the singlet state at their respective equilibrium geometries (which are qualitatively very similar to that of the singlet). Most of the FPD calculations then proceeded assuming a 1A_1 ground state for ThAu_2 , but subsequent X2C-mmF-EOM-CCSD calculations with the DCG Hamiltonian demonstrated that SO coupling was sufficient to yield a triplet ground state for ThAu_2 .

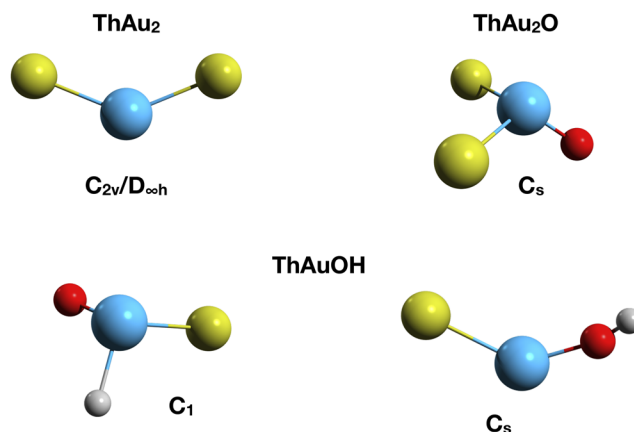


FIG. 3. Lowest energy isomeric structures (thorium in blue, gold in yellow, oxygen in red, and hydrogen in gray).

TABLE I. CCSD(T) equilibrium geometries (Å and deg.) and CCSD(T) harmonic frequencies (cm⁻¹) of the molecules of this work.^{a,b}

$C_{2v}/D_{\infty h}$	ThAu ₂ (¹ A ₁)	ThAu ₂ ⁻ (² Δ _g)
$r(\text{ThAu})$	2.7510	2.8845
θ	136.58	180.00
ω_i	166 (b ₂), 121 (a ₁), 21 (a ₁)	137 (b _{1u}), 89 (a _g), 8 (b _{2u}), 8 (b _{3u})
C_s	ThAu ₂ O (¹ A')	ThAu ₂ O ⁻ (² A')
$r(\text{ThO})$	1.8693	1.8959
$r(\text{ThAu})$	2.8065	2.9185
$\theta(\text{AuThO})$	113.41	109.88
$\phi(\text{AuOThAu})$	132.19	130.07
ω_i	824 (a'), 161 (a''), 127 (a'), 119 (a''), 55 (a'), 25 (a')	780 (a'), 138 (a''), 109 (a'), 90 (a''), 72 (a'), 22 (a')
C_1^c	ThAuOH (¹ A)	ThAuOH ⁻ (² A)
$r(\text{ThO})$	1.8729	1.9028
$r(\text{ThAu})$	2.8081	2.9443
$r(\text{ThH})$	2.1221	2.1841
$\theta(\text{AuThO})$	112.61	111.18
$\theta(\text{HThAu})$	106.96	112.68
$\phi(\text{OAUThH})$	117.21	118.76
ω_i	1454, 822, 472, 226, 142, 79	1281, 770, 374, 242, 119, 88
C_s	ThAuOH (¹ A')	ThAuOH ⁻ (² A')
$r(\text{ThO})$	2.0703	2.1216
$r(\text{ThAu})$	2.7808	2.9530
$r(\text{OH})$	0.9598	0.9564
$\theta(\text{AuThO})$	134.76	165.65
$\theta(\text{ThOH})$	162.59	169.18
ω_i	3880 (a'), 627 (a'), 383 (a'), 346 (a''), 137 (a'), 78 (a')	3922 (a'), 563 (a'), 326 (a'), 320 (a''), 102 (a'), 50 (a')

^aStructures calculated with aVTZ basis sets except for ThAu₂/ThAu₂⁻, which used aVQZ. Harmonic frequencies were calculated with aVDZ basis sets except for ThAuOH/ThAuOH⁻, which used aVTZ.

^bSee also Fig. 3.

^cThe C₁ isomers are the ground states of ThAuOH and ThAuOH⁻.

Combining the SO effect on the state splitting at the EOM-CCSD level with the vertical triplet-singlet splitting at the CCSD(T)/aVTZ level of theory yields a singlet-triplet correction of -1.43 kcal/mol (-0.06 eV). The ground state of the anion has a linear equilibrium geometry with a Th-Au bond length that has lengthened by 0.134 Å upon electron attachment. Relative to the closed-shell ¹A₁ state of the neutral, the additional electron occupies the degenerate 6d_δ orbital on the Th atom, yielding a ²Δ_g ground state. Inclusion of SO coupling results in an Ω = 3/2 ground state (the Ω = 5/2 state lying ~6.6 kcal/mol or 0.29 eV higher in energy at the AoC-DHF level of theory with the DCG Hamiltonian). The results of the FPD

treatment for both the adiabatic EA (EA₀) and VDE are shown in Table II. It can be noted that correlation of the outer-core electrons has a non-negligible effect on the EAs, decreasing EA₀ and VDE by 0.8 and 0.6 kcal/mol, respectively. Including the effects of spin-orbit coupling increases both values by about 4 kcal/mol (0.17 eV). The final FPD value for the adiabatic EA, 29.5 kcal/mol (1.28 eV), which is relative to the triplet ground state of ThAu₂, is in excellent agreement with experiment (1.30 eV).

For ThAu₂⁻, the calculation of the VDE is complicated by the fact that the lowest state of neutral ThAu₂, even at the linear anion geometry, is a ³Δ_{1g} state and not the ¹Σ⁺_{0g} state. At the scalar

TABLE II. Contributions (in kcal/mol) to the FPD adiabatic electron affinity, EA₀, and VDE of ThAu₂. Values in parentheses are in eV.

	aVQZ	ΔCBS	ΔCV	ΔQED	ΔSO	Δ(triplet) ^a	ΔZPE	FPD	Expt. ^b
EA ₀	27.37	+0.14	-0.81	+0.22	+3.91	-1.43	+0.10	29.49 (1.28)	(1.30)
VDE	31.46	+0.29	-0.60	+0.14	+4.15	-1.90	...	33.55 (1.45)	(1.53)

^aSinglet-triplet excitation energy using CCSD(T)/aVTZ and X2C-mmF-EOM-CCSD since the rest of the FPD calculations assumed a singlet ground state for ThAu₂. See the text.

^bThis work.

TABLE III. Electronic excited states of ThAu₂ calculated at the X2C-mmF DCG-EOM-CCSD level of theory using the linear ThAu₂[−] CCSD(T)/aVQZ equilibrium geometry. Values are in eV.

Ω State	dE	VDE	Ω state	dE	VDE
(1) 1 _g	0.00	1.45 ^a	(1) 2 _u	1.768	3.223
(1) 2 _g	0.15	1.60 ^a	(1) 3 _u	1.853	3.308
(1) 0 _g	0.23	1.68 ^a	(1) 0 _u	1.904	3.359
(1) 3 _g	0.38	1.84	(1) 1 _u	1.949	3.404
(2) 0 _g	0.84	2.30	(2) 2 _u	1.969	3.424
(3) 0 _g	0.87	2.32	(2) 0 _u	2.023	3.478
(2) 1 _g	0.90	2.36	(2) 1 _u	2.099	3.554
(2) 2 _g	1.12	2.58	(3) 0 _u	2.336	3.790
(3) 1 _g	1.24	2.70	(3) 2 _u	2.380	3.835
(3) 2 _g	1.33	2.78	(3) 1 _u	2.401	3.856

^aPresumably strong features in the PES since these correspond to 1-electron excitations from the anion ground spin-orbit state. See the text.

relativistic DKH3-CCSD(T)/aVTZ level of theory, the ³Δ_g state lies above the ¹Σ_g⁺ state by 1.99 kcal/mol, but including spin-orbit coupling as the difference between X2C-mmF EOM-CCSD with DCG and SF Hamiltonians favors the Ω = 1_g state over the 0_g spin-orbit state by 3.89 kcal/mol, yielding a final singlet-triplet separation at the anion geometry of −1.90 kcal/mol or −0.08 eV (the triplet being lower). As shown in Table II, this results in a final FPD VDE of 33.6 kcal/mol (1.45 eV), which is in very good agreement with the experimental result (1.53 eV) extracted from the spectrum shown in Fig. 2. The full results of the X2C-mmF DCG-EOM-CCSD calculations at the anion geometry are shown in Table III. Except for the lowest Ω = 0_g state, all of the excited states are dominated by a single excitation from the highest occupied MO of closed-shell ThAu₂, which is predominately Th 7s in character. As shown in Table III, there are many even (g) parity states that might contribute to the PES, particularly the lowest Ω = 1_g, 2_g, and 0_g states that arise from the ³Δ_g and ¹Σ_g⁺ states, respectively. These first 3 Ω states are related to the anion Ω = 3/2 ground electronic state by just a single electron detachment from the 7s orbital and as such might be expected to have relatively strong intensity. (The next excited state of the neutral, the Ω = 3_g, would arise from electron detachment from the SO excited ²Δ_{5/2} state of the anion.) From these calculations though, it is not clear which of these gerade states could be assigned to the PES feature marked “A” at about 2.7 eV. The first ungerade state lies at a VDE of about 3.2 eV.

b. ThAu₂O/ThAu₂O[−]. As seen in Fig. 3, the equilibrium geometries of the ThAu₂O and ThAu₂O[−] molecules have a pyramidal structure with a central Th atom, corresponding to C_s symmetry.

The neutral molecule has a closed-shell MO configuration, and the ground electronic state of the anion involves the attachment of the electron into an MO localized on Th with predominately Th 7s character with contributions from the Th 6d and 7p orbitals. As shown in Table I, the largest change in the ThAu₂O structure upon electron attachment is in the Th–Au bond length, which lengthens by 0.112 Å. The other internal coordinates only involve minor changes. Table IV shows the FPD results for EA₀ and the VDE. In this case, all of the FPD contributions on top of the FC-CCSD(T)/aVQZ values are relatively small. The largest is the effect of including SO coupling, but even this is just −0.90 and −0.59 kcal/mol for the EA₀ and VDE, respectively. This is not surprising since the additional electron occupies primarily a Th 7s orbital. The final FPD result for the EA₀ is 31.3 kcal/mol (1.36 eV), which is in excellent agreement with the experimental value of 1.35 eV. The VDE obtained by FPD, 35.1 kcal/mol (1.52 eV) is, however, lower than the experimental result (1.65 eV) by 0.13 eV. In regard to the features A and B shown in the spectrum of Fig. 2, it is not clear at present what these might correspond to. The results of EOM-CCSD calculations on ThAu₂O (at the anion geometry) show the first two excited states to be triplets and lie about 3 eV above the ground state. The corresponding singlets are higher in energy by about another 0.1 eV. These excitation energies correspond to detachment energies of 4.5 eV and above, which are far above the highest energy portion of the measured PES. A search for alternative structures of the anion that might explain the features at higher binding energies was also attempted but was unsuccessful. Other reasonable clusters having a m/z coincidence with ThAu₂O[−] were also ruled out.

c. ThAuOH/ThAuOH[−]. Initial work on ThAuOH/ThAuOH[−] assumed a bent molecule with a central Th atom in analogy to bent ThF₂ (or ThAu₂). A planar structure with C_s symmetry was readily found, and its structural parameters are given in Table 1. As in the ThAu₂ case, the closed-shell neutral molecule has a highest occupied molecular orbital (HOMO) that is primarily Th 7s in character. The anion is formed by attaching an electron in a Th 6d orbital, yielding a ²A′ electronic state. As in the previous cases considered in this study, the largest change in the neutral structure upon electron attachment is in the Th–Au bond length, which lengthens by 0.172 Å. Some lengthening of the Th–O distance is also observed, 0.051 Å, and the Au–Th–O bond angle opens up by about 30°. As shown in Table V, the calculated EA₀ value is smaller than that of ThAu₂, but the FPD contributions are rather similar with outer-core correlation decreasing the EA by about 1 kcal/mol and SO increasing it by about 3. The final FPD result for EA₀, 20.4 kcal/mol (0.89 eV), is in good agreement with the experimental result of 0.80 eV. The calculated VDE of 24.6 kcal/mol (1.06 eV) is also in very good agreement with the experimental value of 1.03 eV. Both of these results seem

TABLE IV. Contributions (in kcal/mol) to the FPD adiabatic electron affinity, EA₀, and VDE of ThAu₂O. Values in parentheses are in eV.

	aVQZ	ΔCBS	ΔCV	ΔQED	ΔSO	ΔZPE	FPD	Expt. ^a
EA ₀	32.40	−0.02	−0.30	−0.06	−0.90	+0.14	31.26 (1.36)	(1.35)
VDE	35.37	+0.12	+0.38	−0.16	−0.59	...	35.12 (1.52)	(1.65)

^aThis work.

TABLE V. Contributions (in kcal/mol) to the FPD adiabatic electron affinity, EA₀, and VDE of ThAuOH as well the 0 K isomerization energy of ThAuOH⁻ (ΔE_{isom}). Values in parentheses are in eV.

Isomer ^a		aVQZ	ΔCBS	ΔCV	ΔQED	ΔSO	ΔZPE	FPD	Expt. ^b
C ₁	EA ₀	29.58	-0.04	-0.18	-0.04	+0.42	+0.46	30.21 (1.31)	
	VDE	32.12	+0.09	+0.44	-0.11	+0.69	...	33.23 (1.44)	(1.43)
C _s	EA ₀	17.96	+0.10	-1.16	+0.24	+3.04	+0.24	20.41 (0.89)	(0.80)
	VDE	21.64	+0.23	-0.90	+0.20	+3.37	...	24.55 (1.06)	(1.03)
	ΔE _{isom}	39.07	+0.41	+0.44	+0.30	-2.24	+3.44	41.43 (1.80)	

^aSee Fig. 3. The C₁ isomer is in the ground state.^bThis work.

to accurately account for the feature marked X in the spectrum of Fig. 2.

In regard to features A and B of the PES shown in Fig. 2, excited states of the C_s form of ThAuOH were calculated at the CCSD(T)/aVTZ equilibrium geometry of the anion using the X2C-mm-f-EOM-CCSD level of theory. These results are shown in Table VI. Without the inclusion of SO coupling, the low-lying excited states are composed of various singlets and triplets, all of which originate from an excitation from the HOMO of the neutral that has primarily Th 7s character. It is easily seen that the near-linear structure used in these calculations leads to many excited states that are nearly degenerate. The first excited state is calculated to be a ³A'' state and lies within 0.2 eV of the singlet ground state. The next state, a ¹A'' state, is separated by 1 eV, and then, there are many singlet and triplet states separated by only a few tenths of an eV. With the inclusion of SO coupling, one of the components of the lowest ³A'' state is now isoenergetic with the closed-shell ¹A' state. The next two components of the triplet lie within 0.14 and 0.35 eV of the SO ground state. As in the SF case, the next states then begin about 1 eV higher in energy and are all relatively closely

spaced. Referring to the PES of Fig. 2, the width of peak X can now be attributed, in part, to the contributions from up to three electronic states. Peak A could be due, in part, to the excited state with a VDE of 1.4 eV. It is not clear what peak B could be attributed to except perhaps high-lying excited states of ThAuOH.

The relatively large intensity of peak A, however, is difficult to easily rationalize. This led to a search for alternative structures, which led to the C₁ symmetry molecule shown in Fig. 3, which has a central Th atom bonded directly to Au, O, and H. For this isomer, which like ThAu₂O is also formally a Th(IV) species, the anion is formed by attaching an electron to the empty Th 7s orbital of the closed-shell neutral. From the structural parameters given in Table I, electron attachment again leads to large changes in the Th–Au distance (+0.136 Å) and modest elongation of the Th–O distance (+0.030 Å). Most importantly, as shown in Table V, the C₁ isomer of the anion is more stable than the C_s form by 41.4 kcal/mol (1.80 eV). As also shown in Table V, the electron affinity is slightly larger for the C₁ isomer as compared to the C_s one. Just as in ThAu₂O, all the contributions beyond the FC CCSD(T)/aVQZ values are relatively small. The FPD result for the EA₀, 30.2 kcal/mol (1.31 eV), and the VDE, 33.2 kcal/mol (1.44 eV), seem to be good matches for peak A in the PES of Fig. 2. The relatively large intensity could be due to the higher population of the C₁ form relative to the C_s isomer (since it is significantly more stable) but also due to excited state contributions from the latter isomer as mentioned above. In addition, as in the ThAu₂O case, excited states arising from the C₁ isomer are not predicted to play a role in the PES of Fig. 2 since the first excited state (at the anion geometry) is calculated to lie 3.0 eV above the electronic ground state (without SO), which corresponds to a VDE of about 4.5 eV.

TABLE VI. EOM-CCSD (X2C-mm-f) excited electronic states (in eV) for the C_s isomer of ThAuOH at the anion geometry.

State	Without SO		With SO		
	dE	VDE	State	dE	VDE
¹ A'	0.00	1.06	1	0.00	1.06
³ A''	0.16	1.22	2 ^a	0.00	1.07
³ A'	0.16	1.22	3	0.14	1.20
¹ A''	1.16	2.22	4	0.35	1.41
¹ A'	1.16	2.23	5	1.20	2.27
³ A''	1.42	2.48	6	1.33	2.39
³ A'	1.45	2.52	7	1.37	2.43
¹ A''	1.58	2.64	8	1.59	2.65
¹ A'	1.61	2.68	9	1.69	2.75
³ A''	2.16	3.22			
³ A'	2.16	3.22			
³ A''	2.22	3.28			
³ A'	2.24	3.30			

^aThis state corresponds to the closed-shell reference state.

2. Thermochemistry

Atomization energies at 0 K (AE₀s) have been calculated with the FPD method for the neutral molecules of this work to provide additional insights into their bonding. These results, including the breakdown of the FPD contributions, are shown in Table VII. Most of the contributions are relatively large, particularly the effects due to the CBS extrapolation (~3 kcal/mol), outer-core correlation (~5.5 kcal/mol), and SO coupling (~6.5 kcal/mol). The contribution due to the Lamb shift is calculated to be particularly large for ThAu₂, -1.4 kcal/mol, which is about twice as large as the value calculated for ThAu₂O. Generally, this quantity is larger when the change in valence s-orbital occupation is large, which naively would point toward a larger value for ThAu₂O compared to ThAu₂ (see

TABLE VII. Calculated contributions to the FPD 0 K atomization energies (AE_0 s) and resulting heats of formation (all in kcal/mol).

Species	aVQZ	Δ CBS	Δ CV	Δ QED	Δ SO	Δ ZPE	AE_0	H_f (298–0) ^a	ΔH_f (298 K)
ThAu ₂	153.82	+0.83	+5.64	−1.38	−5.83	−0.44	154.1 ^b	+0.67	165.3
ThAu ₂ O	358.55	+2.95	+6.31	−0.71	−7.12	−1.87	358.1	+1.30	20.2
ThAuOH (C ₁)	347.78	+2.87	+4.17	−0.12	−6.68	−4.57	343.5	+2.25	−2.1

^aThermal correction to the atomization energy.^bThis also includes a +1.43 kcal/mol contribution from the singlet–triplet splitting. See the text.

Sec. III). Confirmation of the present results with a more rigorous treatment would be very interesting. The final FPD atomization energy for ThAu₂, 154.1 kcal/mol, which includes a correction for the triplet ground state (see above), is nearly half the AE_0 value of ThF₂.⁶⁷ Curiously, the AE_0 value calculated for ThAu₂O is nearly identical to the sum of the experimental ThO bond dissociation energy (207.6 kcal/mol)⁶⁸ and the ThAu₂ atomization energy. Utilizing experimental heat of formation values for the elements (see Sec. II B), heats of formation at 298 K have been calculated and are also shown in Table VII. The atomization energies have estimated uncertainties of ± 3 kcal/mol, while the heats of formation are estimated at ± 4 kcal/mol due to the uncertainty in the experimental heat of formation of atomic Th (± 1.4 kcal/mol).⁵⁸

3. Electronic structure analysis

Table VIII lists the atomic charges for all the molecules of the present work from natural population analysis. The neutral species are characterized by a positively charged Th atom (between +0.95 and +2.4) with all other atoms negatively charged. In these cases, the charge on Au is about −0.5, while that of O is generally −1.3. In the C₁ isomer of ThAuOH, the H atom is strongly negative with a charge of −0.6. In the anions, the extra electron is localized on Th, so this reduces the positive charge on Th by 0.6 (ThAu₂O) to 0.8 (ThAu₂). The remaining additional negative charge is distributed over the Au and O atoms, although preferentially more on the Au atoms.

The bonding given by NBO analysis is given in Tables IX–XI for ThAu₂, ThAu₂O, and ThAuOH (C₁), respectively. The bonding NBOs of ThAuOH (C₁) are shown in Fig. 4 as representative examples. In all three cases, full sets of 5d lone pairs (10 for ThAu₂ and ThAu₂O and 5 for ThAuOH) are not shown but are also present on the Au atoms. As shown in Table IX for ThAu₂, two σ -type NBOs arise from couplings of Th 7s and 6d natural atomic orbitals (NAOs)

TABLE VIII. Natural charges of ThAu₂, ThAu₂O, and ThAuOH and their anions.

Species	Th	Au	O	H
ThAu ₂ ^a	0.953	−0.477		
ThAu ₂ [−]	0.129	−0.565		
ThAu ₂ O	2.289	−0.517	−1.255	
ThAu ₂ O [−]	1.668	−0.661	−1.347	
(C ₁) ThAuOH	2.391	−0.520	−1.247	−0.624
(C ₁) ThAuOH [−]	1.729	−0.695	−1.348	−0.686
(C _s) ThAuOH	1.340	−0.564	−1.296	0.520
(C _s) ThAuOH [−]	0.561	−0.760	−1.293	0.492

^aThese results are for the singlet state of ThAu₂.

with Au 6s and 5d. The two Th NAOs mix, along with some 7p and 5f character, to form two 6d-rich hybrids (71%) directed toward Au. The Au 7s NAOs remain essentially unhybridized and combine with the Th hybrids to form two σ bonds that are strongly polarized toward the Au atoms with percent ionicities of 58%. The third hybrid on Th is an s-rich (68%) lone pair that arises from mixing the Th 7s and 6d NAOs. For the negative ion, the additional electron occupies an unhybridized 6d orbital on Th and the Th lone pair remains essentially unchanged. The σ bonds become only slightly less d-rich (66%) compared to those of the neutral (71%) with a very similar percent ionicity (55%).

The NBO analysis of the Lewis structure for ThAu₂O shown in Table X consists of one Th–Au bond and three Th–O bonds. The σ bond between Th and Au arises from a hybrid on Th consisting primarily of 7s and 6d NAOs in nearly equal amounts with essentially an unhybridized 6s orbital on Au. This bond is slightly more strongly polarized toward Au than in the ThAu₂ case, as judged by the percent ionicity, 63%. The three bonds between Th and O arise

TABLE IX. NBOs of the Lewis structure for ¹A₁ ThAu₂.^a

NBO	occ	Energy	% ion	c _A	Th hybrid (A)				c _B	Au/O hybrid (B)		
					% s	% p	% d	% f		% s	% p	% d
n_{Th}	1.994	−0.215		1.000	68	2	30	0				
σ_{ThAu}	1.963	−0.349	58.1	0.458	15	9	71	4	0.889	91	0	9

^aThere are also ten lone pairs corresponding to the Au 5d orbitals at energies around −0.46 a.u. Columns include orbital type, occupancy, energy (in au), percent ionicity ($=c_B^2 - c_A^2$), polarization coefficients (c_A and c_B), and percent hybrid character. Bonding NBOs are superpositions of hybrid pairs, $\Omega_{AB} = c_A h_A + c_B h_B$.

TABLE X. NBOs of the Lewis structure for $^1A'$ ThAu₂O.^a

NBO	occ	Energy	% ion	c _A	Th hybrid (A)				c _B	Au/O hybrid (B)		
					% s	% p	% d	% f		% s	% p	% d
σ_{ThAu}	1.969	-0.332	62.6	0.4323	38	7	49	6	0.9017	93	1	6
π_{ThO}	1.983	-0.468	81.6	0.3033	0	1	61	37	0.9529	0	99	1
π_{ThO}	1.999	-0.485	77.6	0.3344	0	0	73	26	0.9424	1	99	1
σ_{ThO}	1.995	-0.816	69.9	0.3877	2	6	63	29	0.9218	23	76	1

^aThere are also ten lone pairs corresponding to the Au 5d orbitals at energies around -0.46 a.u. The 2s lone pair on O is at -0.92 a.u. Columns include orbital type, occupancy, energy (in a.u.), percent ionicity ($=c_B^2 - c_A^2$), polarization coefficients (c_A and c_B), and percent hybrid character. Bonding NBOs are superpositions of hybrid pairs, $\Omega_{AB} = c_A h_A + c_B h_B$.

TABLE XI. NBOs of the Lewis structure for 1A ThAuOH (C₁).^a

NBO	occ	Energy	% ion	c _A	Th hybrid (A)				c _B	Au/O hybrid (B)		
					% s	% p	% d	% f		% s	% p	% d
σ_{ThAu}	1.987	-0.334	61.3	0.4398	47	5	44	4	0.8981	92	1	7
σ_{ThH}	1.990	-0.409	62.6	0.4323	25	2	63	10	0.9017	100	0	0
π_{ThO}	1.998	-0.476	78.0	0.3314	1	0	73	26	0.9435	1	99	1
σ_{ThO}	1.990	-0.589	73.6	0.3635	2	4	65	29	0.9316	15	84	1
π_{ThO}^b	1.990	-0.688	76.6	0.3418	1	2	68	28	0.9398	8	91	1

^aThere are also five lone pairs corresponding to the Au 5d orbitals at energies around -0.46 a.u. Columns include orbital type, occupancy, energy (in a.u.), percent ionicity ($=c_B^2 - c_A^2$), polarization coefficients (c_A and c_B), and percent hybrid character. Bonding NBOs are superpositions of hybrid pairs, $\Omega_{AB} = c_A h_A + c_B h_B$.

^bThis hybrid has a mixture of both σ and π character.

from couplings of Th 6d and 5f NAOs with 2s and 2p NAOs of O. The σ bond involves a d-rich (63%) hybrid on Th mixing with a p-rich hybrid (76%) on O. The two π bonds also involve d-rich hybrids on Th (61% and 73%) but mix with unhybridized 2p orbitals on O. All three bonds are more strongly polarized toward the O atom compared to the Th–Au bond, particularly in the case of the π bonds. In the case of the anion of ThAu₂O, the additional electron occupies a Th s-rich (54%) hybrid lone pair orbital that arises from coupling Th 7s, 7p (22%), and 6d (22%) NAOs. The other NBOs are similar to those of the neutral except that the Th–Au s bond is a bit more rich in d character (66%) compared to the neutral.

An NBO analysis of the bonding in the C₁ isomer of ThAuOH is shown in Table XI. A total of five bonds are formed, σ bonds between Th, Au, and H with σ and π bonds between Th and O. In this sense, the bonding is similar to ThAu₂O. The s bond between Th and Au is from the couplings of 7s and 6d NAOs on Th mixing with primarily an unhybridized 6s on Au. The resulting hybrid on Th has nearly equal parts of 7s (47%) and 6d (44%) with small contributions of 7p and 5f. Not surprisingly, the bond is polarized toward the more electronegative Au atom with a percent ionicity of 61%. The Th–H s bond involves a d-rich (63%) hybrid on Th mixing with the 1s of H. This bond is also very polarized toward H (% ionicity of 63%). Finally, the σ and π bonds between Th and O are very similar to those described previously for ThAu₂O although one of the bonds designated as π is actually a mixture of both σ and π character. The unpaired electron in the negative ion of ThAuOH (C₁) occupies an s-rich (54%) lone pair orbital on Th with strong contributions from p-type (24%) and d-type (19%) NAOs. The other NBOs are

very similar to those of the neutral except that the Th–Au and Th–H σ bonds become more d-rich and more polarized away from the Th.

4. Correspondence of Th–Au and Th–F species

As noted in the Introduction, it has been previously noted that Au⁺ and Au can behave as analogs of O and halogens, respectively. In order to investigate this further, DKH3-CCSD(T)/aVTZ calculations have been carried out on the F-analogs of some of the present molecules, i.e., ThF₂/ThF₂⁻, ThF₂O/ThF₂O⁻, and ThFOH/ThFOH⁻ (C₁). In each of these cases, the ground electronic states were identical to the Au-analogs, and the equilibrium structures were remarkably similar outside of the expected shorter Th–F bond compared to Th–Au. In regard to the equilibrium electron affinities, the F-containing molecules have CCSD(T)/aVTZ EA values [ThF₂: 17.1 kcal/mol, ThF₂O: 28.8 kcal/mol, and ThFOH (C₁): 26.4 kcal/mol] smaller than the analogous Au-containing ones (27.1, 32.5, and 29.7 kcal/mol for ThAu₂, ThAu₂O, and ThAuOH, respectively) by 3–10 kcal/mol, with the largest difference observed for ThF₂. On inspection of the NBOs, the Th–O bonds in ThF₂O and ThFOH are nearly identical in character to those of ThAu₂O and ThAuOH. The Th–F bonds, however, are much more polarized toward F in comparison to Au, and the hybrid orbitals on Th involved in these σ -type bonds have substantial 6d and 5f character with very little s or p contributions. This is particularly true for ThF₂ where the % ionicity of the σ_{ThF} bond is 89.0% compared to 58.1% for σ_{ThAu} , and the % of 5f character is 25% compared to just

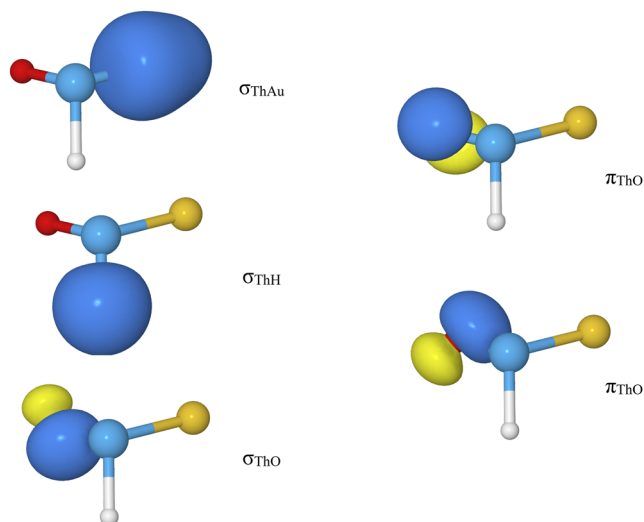


FIG. 4. Bonding NBOs of the ground state of ThAuOH (C_1).

4% for the ThAu₂ case. In the negative ion, ThF₂⁻, the addition of the extra electron into a Th 6d orbital results in the bonding becoming sufficiently ionic that no formal bonds were discovered in the NBO analysis.

IV. CONCLUSIONS

The ThAu₂⁻, ThAu₂O⁻, and ThAuOH⁻ negative ions were characterized both experimentally by anion photoelectron spectroscopy and by *ab initio* calculations based on relativistic coupled cluster theory. Excellent agreement between experiment and theory was observed, to within 0.02 eV, for the adiabatic electron affinities (0 K from theory and the threshold EBE from experiment). In particular, the spectrum of ThAuOH⁻ was interpreted as arising from two isomers, one corresponding to Th(IV) and the other (less stable) to Th(II). The bonds of Th to Au were calculated to be fairly ionic but were not nearly as ionic as Th–F bonds, as indicated by analogous calculations on the F-analogs of these three Au-containing molecules. Atomization energies and heats of formation were calculated for the neutral species using the same composite relativistic coupled cluster methodology as the EAs, yielding expected accuracies of 3–4 kcal/mol.

ACKNOWLEDGMENTS

This work was supported by the U.S. Department of Energy (DOE), Office of Science, Office of Basic Energy Sciences, Heavy Element Chemistry program [Grant Nos. DE-SC0019317 (K.H.B.) and DE-SC0008501 (K.A.P.)].

AUTHOR DECLARATIONS

Conflict of Interest

The authors have no conflicts to disclose.

DATA AVAILABILITY

The data that support the findings of this study are available from the corresponding authors upon reasonable request.

REFERENCES

- 1 J. Vergnes and D. Lecarpentier, *Nucl. Eng. Des.* **216**, 43 (2002).
- 2 V. Jagannathan, *Int. J. Energy Res.* **42**, 117 (2018).
- 3 C. Lombardi, L. Luzzi, E. Padovani, and F. Vettriano, *Prog. Nucl. Energy* **50**, 944 (2008).
- 4 D. Heuer, E. Merle-Lucotte, M. Allibert, M. Brovchenko, V. Ghetta, and P. Rubiolo, *Ann. Nucl. Energy* **64**, 421 (2014).
- 5 Y.-L. Li, X.-G. Xiong, and H.-T. Liu, *Nucl. Sci. Tech.* **30**, 70 (2019).
- 6 J.-B. Liu, X. Chen, J.-B. Lu, H.-Q. Cui, and J. Li, *J. Comput. Chem.* **39**, 2432 (2018).
- 7 Y. Gong, L. Andrews, V. E. Jackson, and D. A. Dixon, *Inorg. Chem.* **51**, 11055 (2012).
- 8 Y. Li, J. Zou, X.-G. Xiong, J. Su, H. Xie, Z. Fei, Z. Tang, and H. Liu, *J. Phys. Chem. A* **121**, 2108 (2017).
- 9 Y. Li, J. Zou, X.-G. Xiong, H. Xie, Z. Tang, M. Ge, Y. Zhao, and H. Liu, *J. Chem. Phys.* **148**, 244304 (2018).
- 10 R. M. Cox, A. Kafle, P. B. Armentrout, and K. A. Peterson, *J. Chem. Phys.* **151**, 034304 (2019).
- 11 T. Tabakova, V. Idakiev, K. Tenchev, F. Boccuzzi, M. Manzoli, and A. Chiorino, *Appl. Catal., B* **63**, 94 (2006).
- 12 Y. Tang, S. Zhao, B. Long, J.-C. Liu, and J. Li, *J. Phys. Chem. C* **120**, 17514 (2016).
- 13 B. Long, Y. Tang, and J. Li, *Nano Res.* **9**, 3868 (2016).
- 14 M. Barysz and P. Pykkö, *Chem. Phys. Lett.* **368**, 538 (2003).
- 15 P. Hrobárik, M. Straka, and P. Pykkö, *Chem. Phys. Lett.* **431**, 6 (2006).
- 16 L. Gagliardi, *J. Am. Chem. Soc.* **125**, 7504 (2003).
- 17 M. Gerhards, O. C. Thomas, J. M. Nilles, W.-J. Zheng, and K. H. Bowen, Jr., *J. Chem. Phys.* **116**, 10247 (2002).
- 18 J. Ho, K. M. Ervin, and W. C. Lineberger, *J. Chem. Phys.* **93**, 6987 (1990).
- 19 S. Burkart, N. Blessing, B. Klipp, J. Müller, G. Ganteför, and G. Seifert, *Chem. Phys. Lett.* **301**, 546 (1999).
- 20 Z. Zhu, M. Marshall, R. M. Harris, K. H. Bowen, M. Vasiliu, and D. A. Dixon, *J. Phys. Chem. A* **125**, 258 (2021).
- 21 H. R. Siekmann, C. Lüder, J. Faehrmann, H. O. Lutz, and K. H. Meiwes-Broer, *Z. Phys. D: At., Mol. Clusters* **20**, 417 (1991).
- 22 X. Zhang, Y. Wang, H. Wang, A. Lim, G. Ganteför, K. H. Bowen, Jr., J. U. Revels, and S. N. Khanna, *J. Am. Chem. Soc.* **135**, 4856 (2013).
- 23 Y. J. Ko, A. Shakyia, H. Wang, A. Grubisic, W. Zheng, M. Götz, G. Ganteför, K. H. Bowen, Jr., P. Jena, and B. Kiran, *J. Chem. Phys.* **133**, 124308 (2010).
- 24 X. Zhang, G. Ganteför, K. H. Bowen, Jr., and A. N. Alexandrova, *J. Chem. Phys.* **140**, 164316 (2014).
- 25 H. Wang, Y. Jae Ko, X. Zhang, G. Ganteför, H. Schnoekel, B. W. Eichhorn, P. Jena, B. Kiran, A. K. Kandalam, and K. H. Bowen, Jr., *J. Chem. Phys.* **140**, 124309 (2014).
- 26 H. Wang, X. Zhang, Y. J. Ko, A. Grubisic, X. Li, G. Ganteför, H. Schnöckel, B. W. Eichhorn, M.-S. Lee, P. Jena, A. K. Kandalam, B. Kiran, and K. H. Bowen, Jr., *J. Chem. Phys.* **140**, 054301 (2014).
- 27 K. Raghavachari, G. W. Trucks, J. A. Pople, and M. Head-Gordon, *Chem. Phys. Lett.* **157**, 479 (1989).
- 28 P. J. Knowles, C. Hampel, and H. J. Werner, *J. Chem. Phys.* **99**, 5219 (1993).
- 29 M. Douglas and N. M. Kroll, *Ann. Phys.* **82**, 89 (1974).
- 30 B. A. Hess, *Phys. Rev. A* **33**, 3742 (1986).
- 31 T. Nakajima and K. Hirao, *J. Chem. Phys.* **113**, 7786 (2000).
- 32 M. Reiher and A. Wolf, *J. Chem. Phys.* **121**, 10945 (2004).
- 33 T. H. Dunning, *J. Chem. Phys.* **90**, 1007 (1989).
- 34 R. A. Kendall, T. H. Dunning, and R. J. Harrison, *J. Chem. Phys.* **96**, 6796 (1992).
- 35 R. Feng, E. D. Glendening, and K. A. Peterson, *J. Phys. Chem. A* **125**, 5335 (2021).

- ³⁶R. Feng and K. A. Peterson, *J. Chem. Phys.* **147**, 084108 (2017).
- ³⁷K. A. Peterson, *J. Chem. Phys.* **142**, 074105 (2015).
- ³⁸D. A. Dixon, D. Feller, and K. A. Peterson, in *Annual Reports in Computational Chemistry*, edited by A. W. Ralph (Elsevier, 2012), Vol. 8, p. 1.
- ³⁹D. Feller, K. A. Peterson, and D. A. Dixon, *J. Chem. Phys.* **129**, 204105 (2008).
- ⁴⁰K. A. Peterson, D. Feller, and D. A. Dixon, *Theor. Chem. Acc.* **131**, 1079 (2012).
- ⁴¹K. A. Peterson and T. H. Dunning, Jr., *J. Chem. Phys.* **117**, 10548 (2002).
- ⁴²W. A. de Jong, R. J. Harrison, and D. A. Dixon, *J. Chem. Phys.* **114**, 48 (2001).
- ⁴³A. Karton and J. M. L. Martin, *Theor. Chem. Acc.* **115**, 330 (2006).
- ⁴⁴D. Feller, K. A. Peterson, and J. G. Hill, *J. Chem. Phys.* **135**, 044102 (2011).
- ⁴⁵J. M. L. Martin, *Chem. Phys. Lett.* **259**, 669 (1996).
- ⁴⁶P. Pyykkö and L.-B. Zhao, *J. Phys. B: At., Mol. Opt. Phys.* **36**, 1469 (2003).
- ⁴⁷K. G. Dyall, *J. Chem. Phys.* **100**, 2118 (1994).
- ⁴⁸L. Visscher and K. G. Dyall, *Atom Data Nucl. Data Tables* **67**, 207 (1997).
- ⁴⁹L. Visscher, T. J. Lee, and K. G. Dyall, *J. Chem. Phys.* **105**, 8769 (1996).
- ⁵⁰J. Sikkema, L. Visscher, T. Saue, and M. Iliaš, *J. Chem. Phys.* **131**, 124116 (2009).
- ⁵¹C. E. Moore, Atomic Energy Levels, NSRDS-NBS 35; Office of Standard Reference Data, National Bureau of Standards, Washington DC, 1971, Vol. 1.
- ⁵²A. Shee, T. Saue, L. Visscher, and A. Severo Pereira Gomes, *J. Chem. Phys.* **149**, 174113 (2018).
- ⁵³J. F. Stanton and R. J. Bartlett, *J. Chem. Phys.* **98**, 7029 (1993).
- ⁵⁴B. Ruscic and D. H. Bross, "Active Thermochemical Tables (ATcT) values based on ver. 1.122r of the Thermochemical Network" (2021), available at ATcT.anl.gov.
- ⁵⁵B. Ruscic, R. E. Pinzon, G. v. Laszewski, D. Kodeboyina, A. Burcat, D. Leahy, D. Montoy, and A. F. Wagner, *J. Phys.: Conf. Ser.* **16**, 561 (2005).
- ⁵⁶B. Ruscic, R. E. Pinzon, M. L. Morton, G. von Laszewski, S. J. Bittner, S. G. Nijssure, K. A. Amin, M. Minkoff, and A. F. Wagner, *J. Phys. Chem. A* **108**, 9979 (2004).
- ⁵⁷J. W. Arblaster, *J. Phase Equilib. Diffus.* **37**, 229 (2016).
- ⁵⁸J. D. Cox, D. D. Wagman, and V. A. Medvedev, *CODATA Key Values for Thermodynamics* (Hemisphere Publishing Corp., New York, 1989).
- ⁵⁹R. J. M. Konings and O. Beneš, *J. Phys. Chem. Ref. Data* **39**, 043102 (2010).
- ⁶⁰F. Weinhold and C. L. Landis, *Valency and Bonding: A Natural Donor–Acceptor Perspective* (Cambridge University Press, 2005).
- ⁶¹A. E. Reed, R. B. Weinstock, and F. Weinhold, *J. Chem. Phys.* **83**, 735 (1985).
- ⁶²NBO 7.0, Theoretical Chemistry Institute, University of Wisconsin, Madison, WI, 2018.
- ⁶³MOLPRO, version 2020.2, a package of *ab initio* programs, H.-J. Werner, P. J. Knowles, G. Knizia, F. R. Manby, M. Schütz, P. Celani, W. Györfy, D. Kats, T. Korona, R. Lindh, A. Mitrushenkov, G. Rauhut, K. R. Shamasundar, T. B. Adler, R. D. Amos, S. J. Bennie, A. Bernhardsson, A. Berning, D. L. Cooper, M. J. O. Deegan, A. J. Dobbyn, F. Eckert, E. Goll, C. Hampel, A. Hesselmann, G. Hetzer, T. Hrenar, G. Jansen, C. Köppl, S. J. R. Lee, Y. Liu, A. W. Lloyd, Q. Ma, R. A. Mata, A. J. May, S. J. McNicholas, W. Meyer, T. F. Miller III, M. E. Mura, A. Nicklass, D. P. O'Neill, P. Palmieri, D. Peng, T. Petrenko, K. Pflüger, R. Pitzer, M. Reiher, T. Shiozaki, H. Stoll, A. J. Stone, R. Tarroni, T. Thorsteinsson, M. Wang, and M. Welborn, see <https://www.molpro.net>.
- ⁶⁴H.-J. Werner, P. J. Knowles, G. Knizia, F. R. Manby, and M. Schütz, *Wiley Interdiscip. Rev.: Comput. Mol. Sci.* **2**, 242 (2012).
- ⁶⁵H.-J. Werner, P. J. Knowles, F. R. Manby, J. A. Black, K. Doll, A. Hesselmann, D. Kats, A. Köhn, T. Korona, D. A. Kreplin, Q. Ma, T. F. Miller III, A. Mitrushchenkov, K. A. Peterson, I. Polyak, G. Rauhut, and M. Sibaev, *J. Chem. Phys.* **152**, 144107 (2020).
- ⁶⁶DIRAC, a relativistic *ab initio* electronic structure program, release DIRAC19 (2019), written by A. S. P. Gomes, T. Saue, L. Visscher, H. J. Aa. Jensen, and R. Bast, with contributions from I. A. Aucar, V. Bakken, K. G. Dyall, S. Dutilleul, U. Ekström, E. Eliav, T. Enevoldsen, E. Faßhauer, T. Fleig, O. Fossgaard, L. Halbert, E. D. Hedegård, T. Helgaker, B. Helmich-Paris, J. Henriksson, M. Iliaš, Ch. R. Jacob, S. Knecht, S. Komorovský, O. Kullie, J. K. Lærdahl, C. V. Larsen, Y. S. Lee, H. S. Nataraj, M. K. Nayak, P. Norman, G. Olejniczak, J. Olsen, J. M. H. Olsen, Y. C. Park, J. K. Pedersen, M. Pernpointner, R. Di Remigio, K. Ruud, P. Salek, B. Schimmelpfennig, B. Senjean, A. Shee, J. Sikkema, A. J. Thorvaldsen, J. Thyssen, J. van Stralen, M. L. Vidal, S. Villaume, O. Visser, T. Winther, and S. Yamamoto, available at <http://dx.doi.org/10.5281/zenodo.3572669>, see also <http://www.diracprogram.org>.
- ⁶⁷D. L. Hildenbrand and K. H. Lau, *Pure Appl. Chem.* **64**, 87 (1992).
- ⁶⁸R. J. M. Konings, O. Beneš, A. Kovács, D. Manara, D. Sedmidubský, L. Gorokhov, V. S. Iorish, V. Yungman, E. Shenyavskaya, and E. Osina, *J. Phys. Chem. Ref. Data* **43**, 013101 (2014).